

# Anthropogenic impacts on twentieth-century ENSO variability changes

Wenju Cai ® <sup>1,2</sup> ⋈, Benjamin Ng ® <sup>2</sup>, Tao Geng ® <sup>1,3</sup>, Fan Jia ® <sup>4</sup>, Lixin Wu ® <sup>1,3</sup> ⋈, Guojian Wang ® <sup>1,2</sup>, Yu Liu ® <sup>5</sup>, Bolan Gan ® <sup>1,3</sup>, Kai Yang ® <sup>6</sup>, Agus Santoso ® <sup>2,7</sup>, Xiaopei Lin ® <sup>1,3</sup>, Ziguang Li ® <sup>1,3</sup>, Yi Liu<sup>1</sup>, Yun Yang ® <sup>8</sup>, Fei-Fei Jin ® <sup>9</sup>, Mat Collins ® <sup>10</sup> & Michael J. McPhaden ® <sup>11</sup>

#### Abstract

El Niño/Southern Oscillation (ENSO) sea surface temperature (SST) variability increased after 1960, influenced by more frequent strong El Niño and La Niña events. Whether such changes are linked to anthropogenic warming, however, is largely unknown. In this Perspective, we consider anthropogenic impacts on ENSO variability in several commonly used modelling designs, which collectively suggest a greenhouse warming-related effect on post-1960 ENSO SST variability. Specifically, a comparison of simulated ENSO SST variability between 1901–1960 and 1961–2020 indicates that more than three quarters of climate models produce an amplitude increase in post-1960 ENSO SST variability, translating into more frequent strong El Niño and La Niña events. Multiple large ensemble experiments further confirm that the simulated post-1960 ENSO amplitude increase (approximately 10%) is not solely due to internal variability. Moreover, multicentury-long simulations under a constant pre-industrial CO<sub>2</sub> level suggest that the observed post-1960 ENSO variability is high, sitting in the highest 2.5 and 10 percentiles for eastern Pacific and central Pacific ENSO, respectively. Improvement in model ENSO physics, identification of consistent future and historical change in additional ENSO characteristics and single-forcing large-ensemble experiments are further needed to ascertain climate change impacts on the ENSO.

#### **Sections**

Introduction

Consensus in model democracy approach

Consensus in large ensemble experiments

Emerging from baseline variability

Explaining ENSO variability changes

Towards projected ENSO enhancement

Summary and future perspectives

A full list of affiliations appears at the end of the paper. Me-mail: Wenju.cai@csiro.au; Lxwu@ouc.edu.cn

#### Introduction

The El Niño/Southern Oscillation (ENSO) is characterized by two distinctive regimes<sup>1-5</sup>: eastern Pacific ENSO (EP-ENSO), wherein sea surface temperature (SST) anomalies are centred in the equatorial eastern Pacific, with notably strong El Niño (warm) events in comparison to La Niña (cold) events; and central Pacific ENSO (CP-ENSO), wherein SST anomalies are centred in the central equatorial Pacific, with stronger La Niña events in comparison to El Niño. These changes in SST drive anomalous atmospheric convection, leading to large-scale reorganization of the Walker Circulation and shifts in the intertropical convergence zone<sup>6</sup>.

As a result, ENSO describes the most consequential year-to-year fluctuation of the climate system<sup>7-11</sup>. It drives considerable impacts that include El Niño-related droughts in western Pacific regions, floods in eastern Pacific regions<sup>7,10,11</sup> and severe food shortage and cyclones to Pacific Island countries<sup>12-14</sup>; La Niña generally has the opposite impacts. Beyond the tropical Pacific, ENSO affects Southern Ocean winds, upwelling and Antarctic shelf ocean and atmosphere circulation<sup>15,16</sup>, modifying Antarctic sea ice and affecting ice sheet melt<sup>17</sup>.

Observations, aggregated across multiple reanalysis products, suggest that ENSO variability might have changed over the course of the twentieth and twenty-first centuries 18-20. In particular, when comparing 1901–1960 and 1961–2020, the E-index and C-index (representing indices for EP-ENSO and CP-ENSO, respectively) exhibit 31.8% (from 0.88) to 1.16) and 17.9% (from 0.95 to 1.12) increases in variance, respectively (Fig. 1a,b). The increase in *E*-index variability is associated with greater frequency of strong EP-El Niño events (from two events to four events) (Fig. 1c,d). By contrast, the increase in C-index variability reflects the greater frequency of strong La Niña years (from one to nine events), with only a comparatively small increase in the frequency of CP El Niño events (from 11 to 14 events) (Fig. 1d). The increase in ENSO variability is largely consistent across reanalysis data sets (Fig. 1e,f). Palaeo-based analyses further suggest an increase in CP-ENSO and EP-ENSO variability relative to the pre-industrial era, including a ~25% intensification of over-arching ENSO variability during the late-twentieth century relative to the preindustrial period or distant past<sup>21-27</sup>. Thus, reanalysis and palaeo-based analyses suggest that anthropogenic greenhouse gas forcing might have already contributed to an increase in ENSO variability.

The potential influence of anthropogenic warming on observed ENSO is also increasingly corroborated by projections of future ENSO SST variability under rising greenhouse gas emissions. Although there was no intermodel consensus using a conventional SST index at a fixed location<sup>28–31</sup>, in part owing to a strong masking by internal variability, particularly early in the twenty-first century<sup>32–34</sup>, internal variability was suggested to conspire with greenhouse warming to intensify extreme eastern and central Pacific El Niño since 1980 (ref. 35). Yet, the level of intermodel consensus increases with model realism in simulating distinctive CP-ENSO and EP-ENSO; furthermore, a majority of models participating in the sixth phase of the Coupled Model Intercomparison Project<sup>36</sup> (CMIP6) (Supplementary information) simulate an ENSO SST variability increase over the twenty-first century<sup>20,37–39</sup>, reinforcing the potential role of climate change in the observed ENSO change.

However, determining the impact of anthropogenic warming on the observed ENSO SST variability is hampered by uncertainty arising from decadal to multidecadal fluctuations of ENSO, by low-quality data before the 1950s owing to sparse observations and sampling errors  $^{40}$  and by large uncertainties in palaeo-reconstructions  $^{41}$ . Indeed, even if the observations are perfect in quality, the data are too short for an assessment of the possible internal variability range. Yet, determining the anthropogenic contributions to changing ENSO variability is vital

to attribute causes of extreme events that are becoming more frequent and severe  $^{42}$  , to understand ENSO projection and to gauge urgency of mitigation actions.

In this Perspective, we assess the possible impact of greenhouse warming on observed ENSO SST variability under three commonly used approaches with outputs from CMIP6 models. First, a 'one experiment each model' approach, referred to as 'model democracy', wherein only one experiment from each participating model is included in a multimodel ensemble assessment to quantify the change and its multimodel consensus. Second, single-model large ensemble experiments (in which uncertainty is due to internal variability rather than different model structures) are used to determine interexperiment agreement and quantify changes after internal variability is removed. Third, multicentury-long experiments under constant pre-industrial CO<sub>2</sub> forcing (piControl) are used to examine how unusual post-1960 ENSO variability is. The mechanisms underpinning an increase in post-1960 ENSO variability are subsequently discussed, before ending with an emerging picture on contemporary and future ENSO changes and recommendations for future research.

## Consensus in model democracy approach

Assuming that each model is independent and equally valid, the model democracy approach uses only one experiment from each model (Supplementary information), avoiding dominance by models with many experiments<sup>42</sup>; each model is represented equally in the assessment of intermodel consensus and the ensemble mean change. Here, 43 CMIP6 models<sup>36</sup> are used, each forced with observed historical emissions of greenhouse gases to 2014 and the Shared Socioeconomic Pathways 585 (SSP585) to 2020. The full 120 years of 1901–2020 are divided into the two longest possible equal-length 60-year subperiods, maximizing the climate change signal but minimizing the influence of internal variability<sup>43</sup>.

Previous research has heavily utilized this approach to examine ENSO change. Indeed, the model democracy method demonstrates intermodel consensus on increased ENSO variability from the twentieth to the twenty-first century in key characteristics of ENSO. These include an increased frequency of eastward propagating El Niño events44; increased ENSO-related extreme rainfall variability, even if ENSO SST variability does not change 12,14,20,45-48; increased SST variability in the equatorial central Pacific (Niño4 region), translating to an increased frequency of extreme La Niña<sup>37,49</sup> and enhanced EP-ENSO SST variability at anomaly centres unique to individual models<sup>50</sup> in models with more realistic ENSO diversity and nonlinearity. The increased variability of EP-ENSO and CP-ENSO is associated with more occurrences of extreme EP El Niño and extreme La Niña events, and in swings from an extreme EP El Niño in a year to an extreme La Niña the next year<sup>37</sup>. Compared with CMIP5 (ref. 51), CMIP6 models have generally improved in simulating extreme ENSO events and their linkage, and the projected increase in ENSO SST variability is simulated in a greater majority of models<sup>20,52</sup>. Niño3.4, for example, which represents CP-ENSO and EP-ENSO combined, exhibits increased ENSO variability in the majority of CMIP6 models<sup>39</sup>.

This model democracy approach also demonstrates strong intermodel consensus on strengthened post-1960 ENSO variability, encompassing more frequent strong El Niño and strong La Niña events. Specifically, 33 out of 43 models (-77%) simulate an increased E-index standard deviation, with a multimodel ensemble increase of  $6.9 \pm 1.4\%$  (Fig. 2a), statistically significant above the 95% confidence level (Supplementary information). The increase in E-index standard

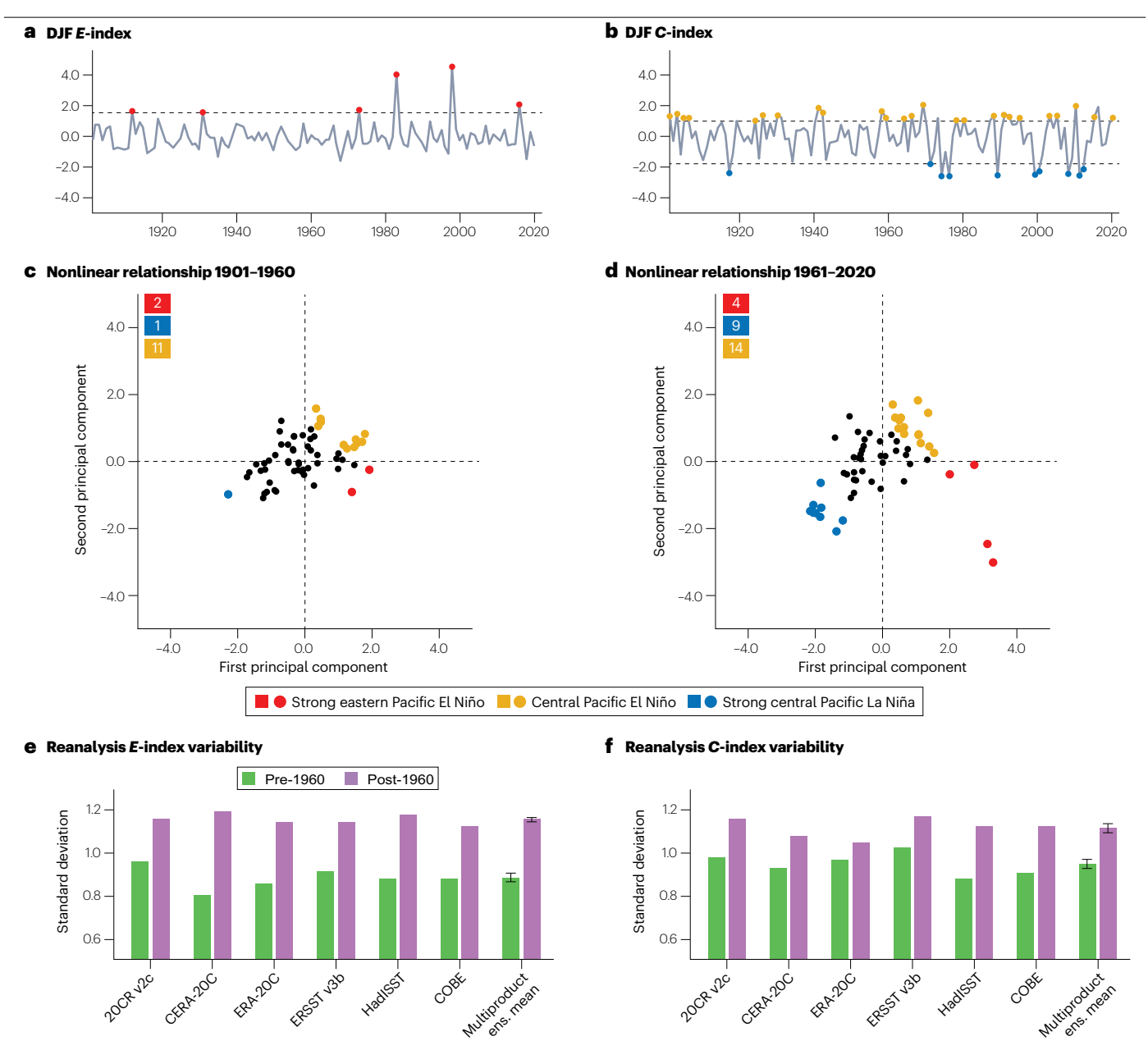


**Fig. 1** | **Observed** *E***-index and** *C***-index from 1901 to 2020. a**, Mean December–January–February (DJF) *E*-index from monthly time series averaged across six individual reanalysis data sets <sup>88–93</sup>. **b**, As in part **a**, but for the *C*-index. **c**, Nonlinear relationship between the first and second principal components of equatorial Pacific sea surface temperature (SST) for the 1901–1960 period. Strong eastern Pacific El Niño events (red) are defined as events wherein the DJF-averaged *E*-index is greater than 1.5 standard deviations. Central Pacific El Niño events (yellow) are defined as events wherein the *C*-index is greater than 1.0 standard deviations. Strong La Niña events (blue) are defined as events wherein the negative *C*-index has amplitude greater than 1.75 standard

deviations. Numbers indicate the frequency of each type of event. **d**, As in part **c**, but for 1961–2020. **e**, *E*-index standard deviation from the six different reanalysis products<sup>88–93</sup>, with the green and purple bars indicating the pre-1960 and post-1960 periods, respectively. **f**, As in part **e**, but for the *C*-index. The multiproduct mean is the average of the standard deviations from the six products, with error bars representing the two standard deviation values of interproduct variability. Although observations suggest an increase in El Niño/Southern Oscillation variability post-1960, the possibility that such changes are due to internal variability cannot be excluded, even if data quality is not an issue.

deviation is  $6.2 \pm 1.6\%$ , supported by 27 out of 43 models (62.8%) (Fig. 2b). Correspondingly, there is a multimodel average of 55.1% increase in the frequency of strong EP El Niño events and a 59.7% increase in years of

strong La Niña (Fig. 2c,d), both statistically significant; there is a slight decrease in CP-El Niño events that is not statistically significant. An intermodel consensus (-77%) on the increase in post-1960 ENSO is

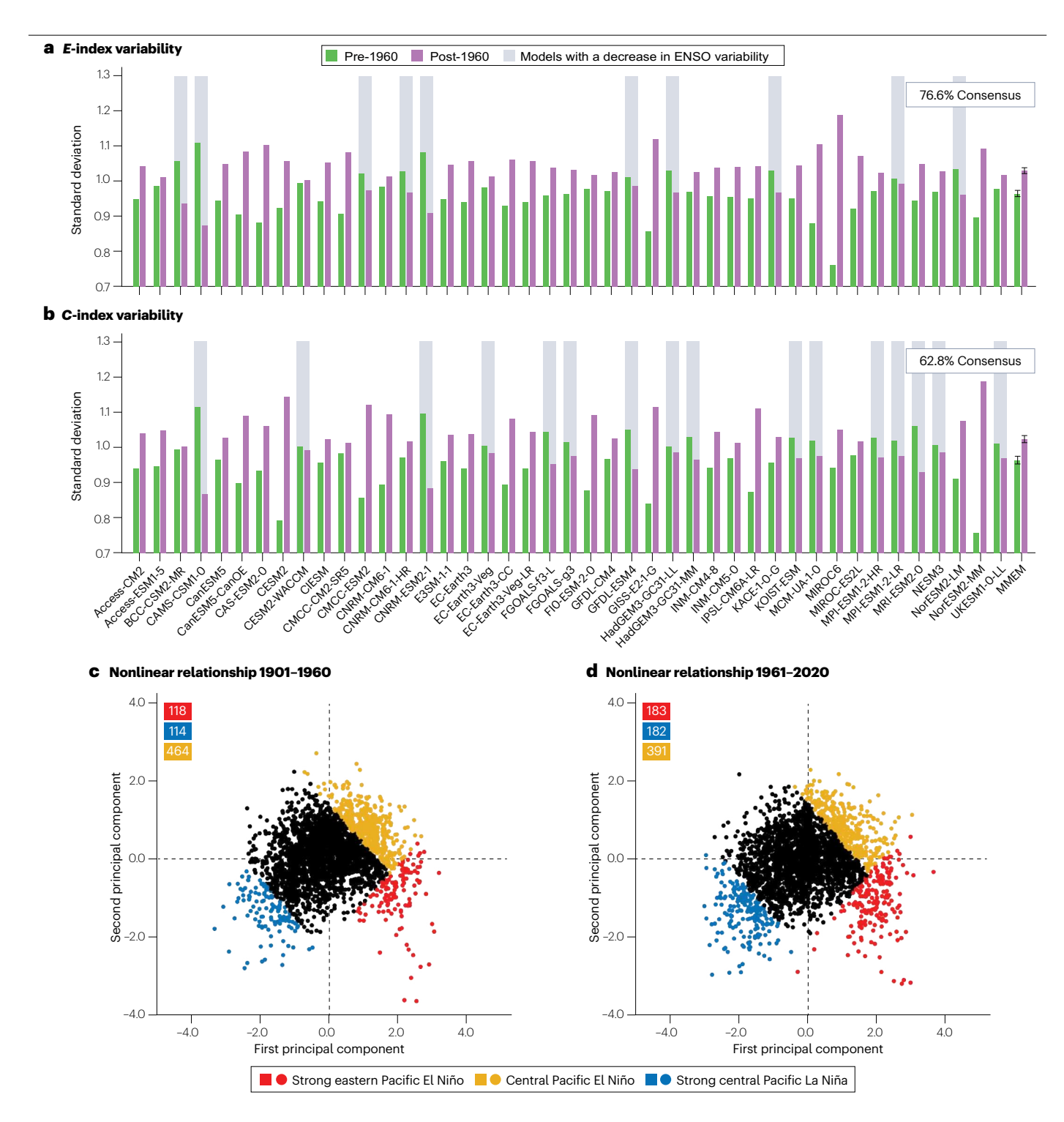


**Fig. 2** | **Simulated increase in post-1960 El Niño/Southern Oscillation variability. a**, E-index standard deviation for the 1901–1960 (green) and 1961–2020 (purple) periods from 43 available Coupled Model Intercomparison Project 6 models  $^{36}$ . The grey shading indicates models that do not simulate an increase in El Niño/Southern Oscillation (ENSO) variability, with the percentage of models that simulate an increase denoted on the top right. **b**, As in part **a**, but for the E-index. **c**, Nonlinear relationship between the first and second principal components of equatorial Pacific sea surface temperature for the

 $1901-1960\ period.\ Strong\ La\ Niña\ (blue),\ central\ Pacific\ El\ Niño\ (yellow)\ and\ strong\ eastern\ Pacific\ El\ Niño\ events\ (red)\ are\ defined\ as\ in\ Fig.\ 1,\ with\ numbers\ indicating\ the\ frequency\ of\ each\ type\ of\ event.\ d,\ As\ in\ part\ c,\ but\ for\ 1961-2020.$  With a model democracy approach, the majority\ of\ models\ reproduce\ the\ observed\ increase\ in\ the\ post-1960\ ENSO\ variability,\ featuring\ an\ increased\ frequency\ of\ strong\ El\ Niño\ and\ strong\ La\ Niña\ events\ MMEM,\ multimodel\ ensemble\ average.

also seen in the Niño3.4 index (Supplementary Fig. 1), grid-point SST variability (Supplementary Fig. 2) or using 50-year instead of 60-year periods to calculate variability (Supplementary Fig. 3).

Thus, models under observed climate change forcing reproduce a post-1960 increase in E-index variability with an increased frequency of strong El Niño and increased C-index variability with an increased frequency of strong La Niña, consistent with the projected change for the future climate  $^{20,38,50}$ . The post-1960 increase in variability is simulated even though each model has unique, independent internal variability, as well as contrasting model physics. However, the intermodel spread

in variability change is large, ranging from -21.1% to 56.2% for E-index and from -22.1% to 56.7% for C-index. Internal variability is found to substantially impact the spread in ENSO change under global warming  $^{33,34,53-56}$ . It is therefore important to assess the intermodel difference after internal variability is removed.

## Consensus in large ensemble experiments

The large spread in the model democracy approach confounds uncertainties from different sources <sup>57,58</sup>, including model structure and internal variability from natural processes that operate even without climate

## a E-index in seven large ensembles 1.8 -Increase 1.5 1.2 961-202C 0.9 Decrease 0.6 0.3 0.0 0.3 0.9 1.5 0.6 1.2 1901-1960



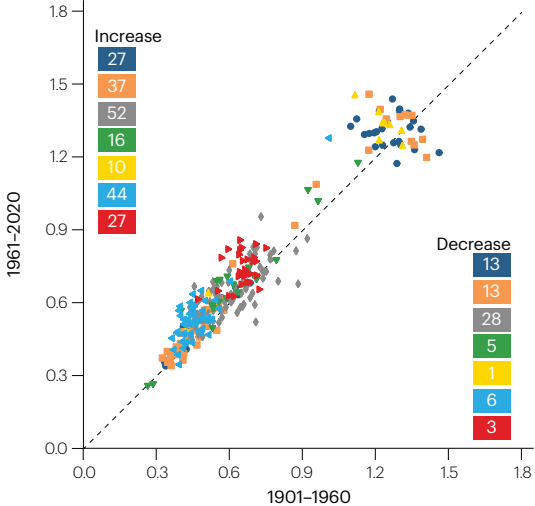
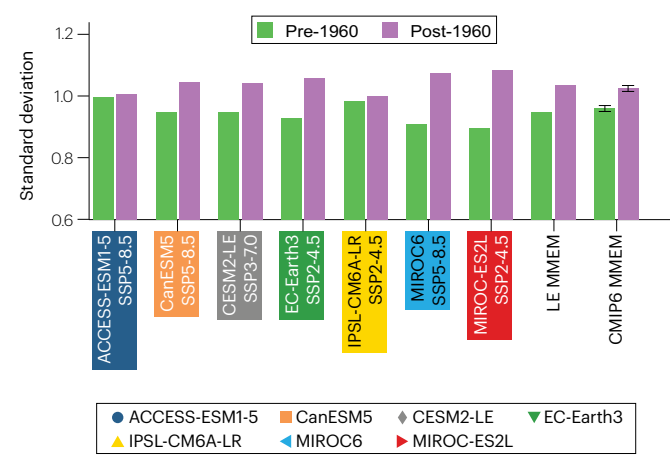
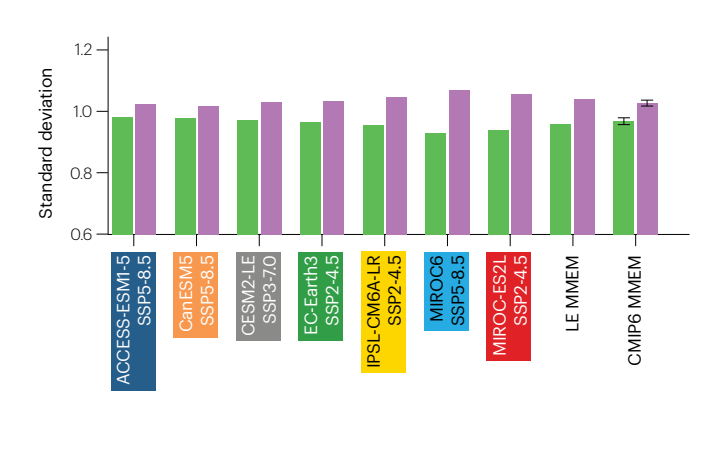


**Fig. 3** | **Increased post-1960 El Niño/Southern Oscillation variability in butterfly-effect ensembles.** a, E-index variability for 1901–1960 versus 1961–2020 for large ensembles in seven models (Supplementary Table 1). The number of experiments in each model producing an increase or a decrease in post-1960 El Niño/Southern Oscillation variability is indicated in the top left and bottom right, respectively, with colours corresponding to the different models. **b**, Large ensemble mean E-index variability in the pre-1960 (green) and the post-1960 (purple) 60-year periods. The E-index for each ensemble experiment is standardized over the 1901–2020 period before calculating the ensemble

## **b** E-index change owing to greenhouse warming



#### d C-index change owing to greenhouse warming



average. The mean across the seven large ensemble averages is represented as large ensemble (LE) and the multimodel ensemble average (MMEM) across all Coupled Model Intercomparison Project 6 (CMIP6) models in the model democracy approach as CMIP6 MMEM; error bars in the latter represent the  $\pm 1.0$  standard deviation range using a Bootstrap method.  ${\bf c}$ , As in part  ${\bf a}$ , but for the C-index.  ${\bf d}$ , As in part  ${\bf b}$ , but for the C-index. Without the influence from internal variability, all seven large ensemble models generate a post-1960 increase in El Niño/Southern Oscillation variability.

change forcing. Uncertainty due to internal variability can be removed by creating a large ensemble of simulations with each climate model under identical climate change forcing through an infinitesimal perturbation to the initial condition of each experiment (Supplementary information). The perturbation creates diverging, randomly phased and independent trajectories of ENSO<sup>59-62</sup>. As such, the forced change can be quantified by averaging over the experiments to remove the influence from internal variability and assessed for an interexperiment consensus. To remove the impact of internal variability, at least 30-40 members are needed when using two 30-year periods to depict the projected change<sup>34</sup>, decreasing to 15 experiments when two 50-year periods are used<sup>33</sup>. Importantly, the number of experiments required decreases with a longer period used to determine the change<sup>53</sup>. Seven available CMIP6 large ensemble experiments are used from models with at least ten experiments and initiated from a time before 1900 and under historical forcing to 2014 (Supplementary Table 1); for the 2015–2020 period and beyond, an emission scenario in each model is chosen, which provides the largest number of experiments.

Previously, it has been demonstrated that the interexperiment range of ENSO variability change between the twentieth century and twenty-first century can be as large as the entire range in the multimodel spread \$33,34,55,56\$ or more than 80% of the spread using two 30-year periods to depict the projected change \$^34\$. Even in a multicentury-long experiment without external forcing, ENSO variability can be vastly different \$^33\$. That internal variability could confound the projected change is illustrated in a case in which the model democracy approach produces no intermodel consensus, but removing the impact of internal variability in each participating model through averaging their respective butterfly-effect ensemble experiments generates an intermodel consensus and a statistically significant change \$^44\$.

Should greenhouse warming not have an impact, it can be expected that approximately 50% of butterfly-effect experiments simulate greater ENSO variability post-1960 than pre-1960. However, in the CMIP6 large ensembles, 225 out of 282 (79.8%) experiments produce an increase in *E*-index (Fig. 3a), unlikely to be from chance. Multi-experiment averages for each model, each having the impact of internal variability removed, similarly indicate a strong intermodel consensus for increased *E*-index variability (Fig. 3b). These features are further evident for the *C*-index (Fig. 3c,d), wherein 75.5% of the experiments generate increased variability, as well as for Niño3.4 (Supplementary Fig. 4), wherein 82.3% of the experiments generate increased variability. Moreover, these changes are robust to changes in the length of periods that are compared (Supplementary Fig. 5).

From the multi-experiment averages in the respective individual models, a multimodel mean *E*-index and *C*-index can be calculated for each period. These indicate variability increases of 10.6% and 8.3% for the *E*-index and *C*-index, respectively, larger than the 6.9% and 6.2% increase suggested by the model democracy approach. Furthermore, the intermodel range is far smaller: 0.7–20.4% for the *E*-index and 4.2–15.0% for the *C*-index, compared with 2.4–56.2% and 3.9–44.4% from the equivalent seven models in the model democracy approach. Thus, higher post-1960 ENSO variability apparent in the model democracy approach is, in part, contributed by anthropogenic warming. In particular, once internal variability is removed, the increase in *C*-index variability, unclear in the model democracy approach, manifests clearly.

## **Emerging from baseline variability**

Another approach to assess the impact of greenhouse warming on ENSO is to determine whether ENSO emerges from a probability distribution in a baseline period without influence of greenhouse warming <sup>43,63</sup>.

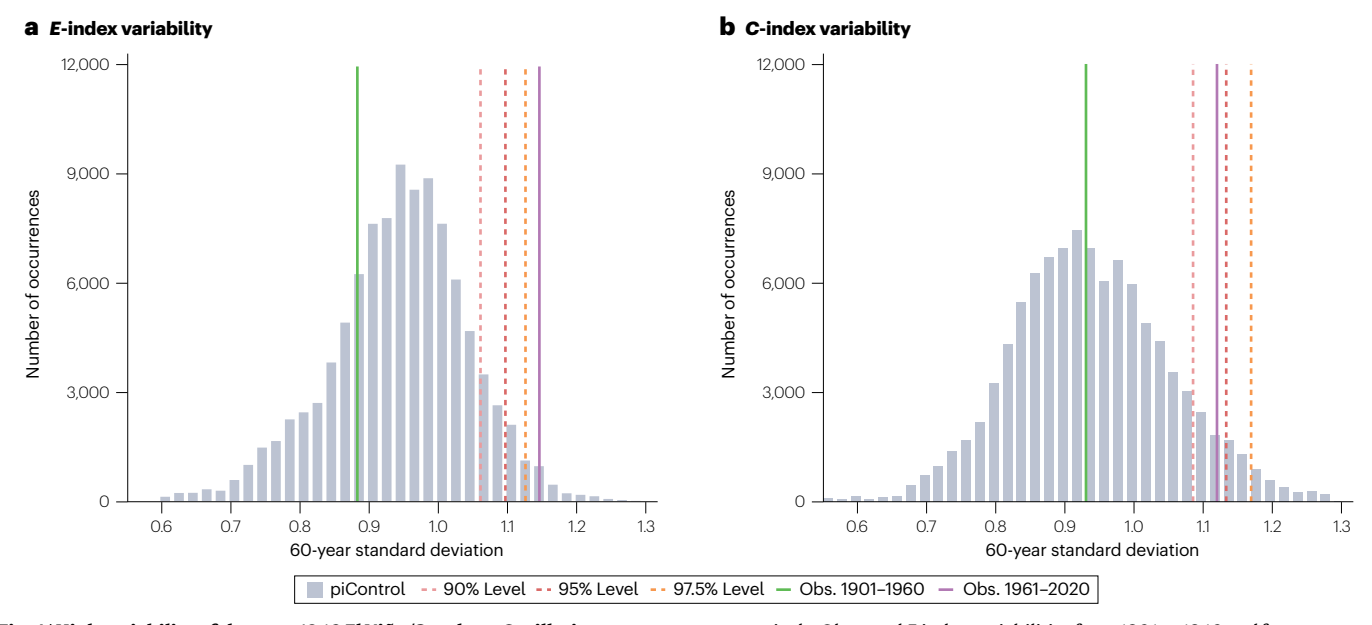


**Fig. 4** | **High variability of the post-1960 El Niño/Southern Oscillation. a**, Histogram of 100,000 realizations of a Bootstrap method for 60-year running standard deviation of E-index in piControl from 39 Coupled Model Intercomparison Project 6 models under a pre-industrial level of constant  $CO_2$  (Supplementary information). The dashed light pink, dark pink and orange lines indicate the upper 10th, 5th and 2.5th percentile values of the histogram,

respectively. Observed E-index variabilities from 1901 to 1960 and from 1961 to 2020, averaged from multiple reanalysis data sets, are shown in solid green and purple lines, respectively.  $\mathbf{b}$ , Same as part  $\mathbf{a}$ , but for the C-index. The observed post-1960 El Niño/Southern Oscillation amplitude is unusually high, sitting within the highest 2.5th and 10th percentile for the E-index and C-index, respectively.

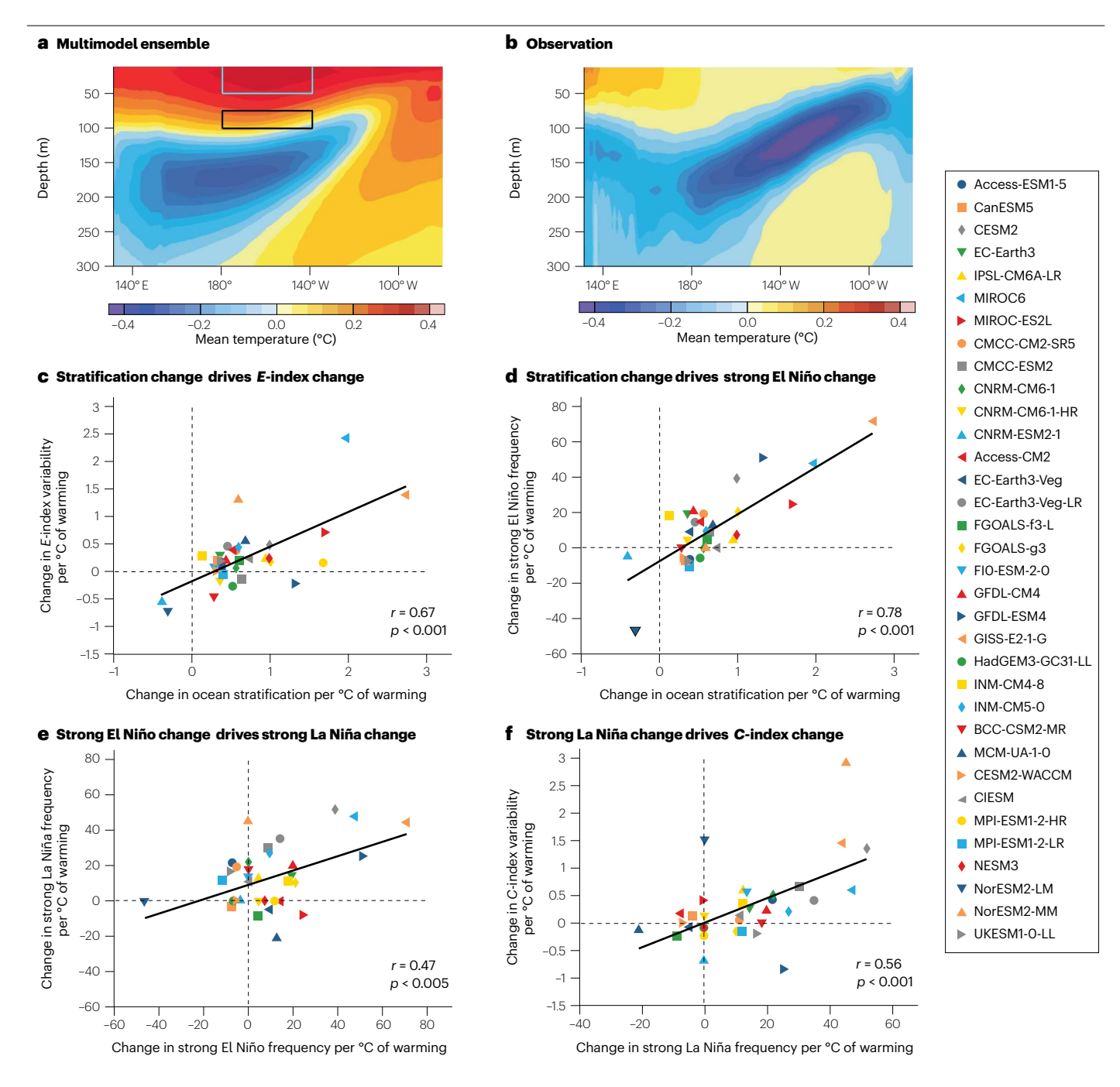
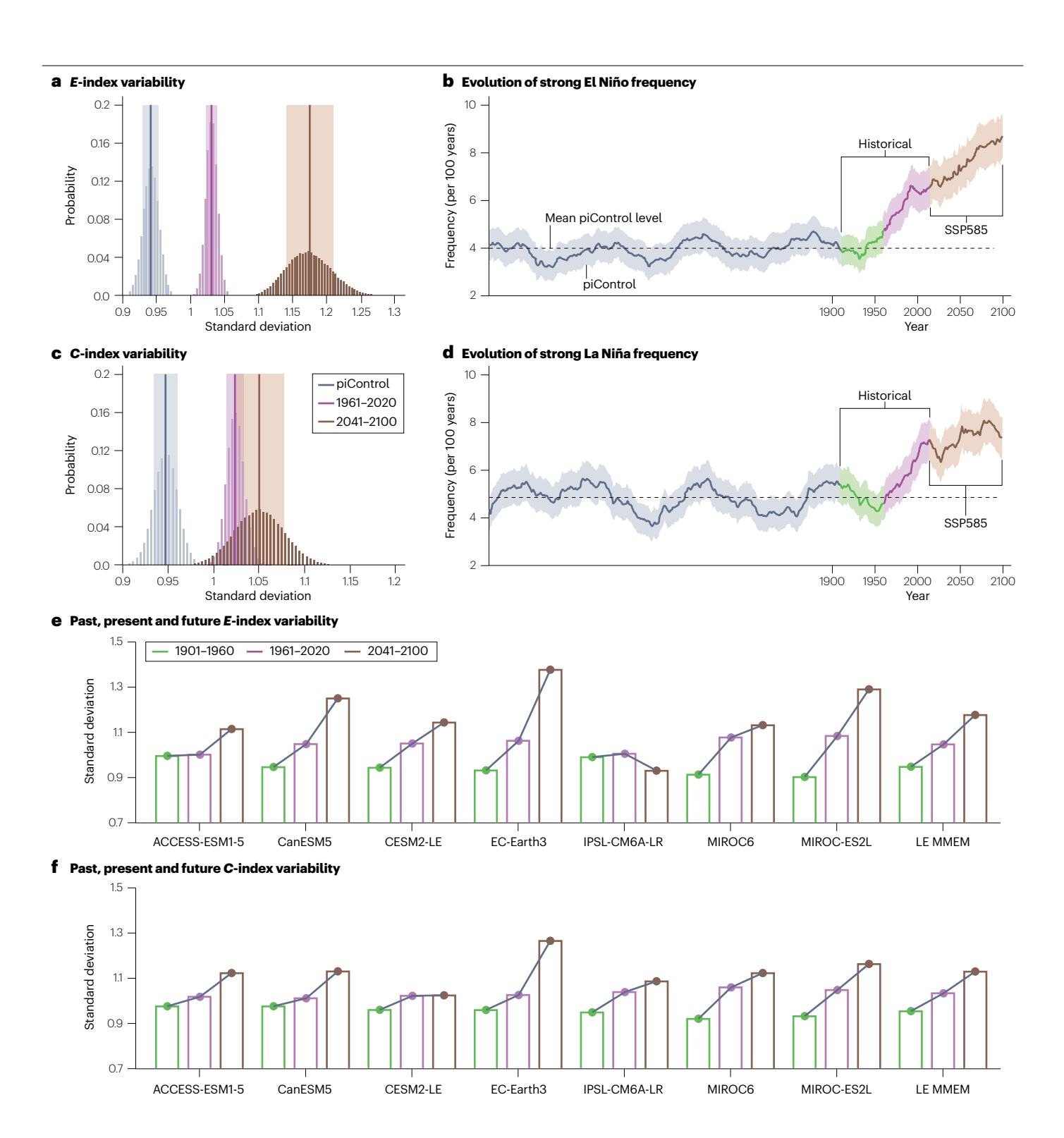


**Fig. 5** | Changes in ocean stratification and in El Niño/Southern Oscillation variability. a, Multimodel ensemble averaged difference in mean ocean temperature warming between the 1961–2020 and 1901–1960 periods, from the 34 Coupled Model Intercomparison Project 6 (CMIP6) models; the light blue and black boxes indicate the regions used to calculate the change in ocean stratification in parts  ${\bf c}$  and  ${\bf d}$ .  ${\bf b}$ , Observed ocean temperature trend (°C per decade) over 1958–2017 averaged from ORA-S3 and ORA-S4 (refs. 74,75).  ${\bf c}$ , Intermodel relationship between the change in ocean stratification and the change in  ${\it E}$ -index standard deviation for 34 CMIP6 models (symbols) in which ocean temperature data are available. Change represented as 1961–2020 minus 1901–1960. A linear fit (solid black line) is displayed together with the correlation coefficient  ${\it R}$  and the corresponding  ${\it p}$ -value.  ${\bf d}$ , As in part  ${\bf c}$ , but

for intermodel relationship between change in ocean stratification and change in the frequency (events per 100 years) of strong El Niño events. **e**, As in part **d**, but for intermodel relationship between the change in frequency (events per 100 years) of strong El Niño events and the change in frequency (events per 100 years) of strong La Niña events. **f**, As in part **c**, but for intermodel relationship between the change in frequency (events per 100 years) of strong La Niña events and the change in C-index standard deviation. All changes in *E*-index, *C*-index and ocean stratification have been scaled by the global sea surface temperature warming in each model between the two 60-year periods. Post-1960 increases in upper-ocean stratification along the equatorial Pacific Ocean intensify ocean–atmosphere coupling, leading to the simulated increase in the post-1960 El Niño/Southern Oscillation amplitude.



In effect, the baseline distribution ('noise') measures the range of natural fluctuations from internal variability, which can be compared with ENSO in a specific period to assess how unusual ENSO variability is during that time – essentially whether a signal emerges permanently out of the range of the noise  $^{53}$  (Supplementary information). The baseline distribution is diagnosed from multicentury-long piControl

experiments  $^{43,63}$ , which, for CMIP6, are available from 39 climate models considered in the model democracy approach (Supplementary Table 2).

To date, the consensus using such an approach is that green-house warming-induced changes in tropical Pacific mean temperature and mean rainfall, or in variability of ENSO SST and rainfall, are uncertain and vastly different across models, with a large intermodel

**Fig. 6** | **Continued increase of El Niño/Southern Oscillation variability into the future.** a, Histogram of 100,000 realizations of a Bootstrap method on 60-year running standard deviation of E-index in piControl (grey bars) and E-index standard deviation in the 1961-2020 (purple bars) and the 2041-2100 (brown bars) periods, respectively, from the 39 Coupled Model Intercomparison Project 6 models that have at least 300 years of piControl. Solid lines and shadings indicate multimodel mean and 1.0 standard deviation of the 100,000 inter-realizations, respectively. **b**, Evolution of strong El Niño frequency (events per 100 years) simulated over a period from piControl to 2100, diagnosed in 60-year sliding windows moving forward from the start of the past 300 years of piControl (black), covering the entire historical period (green and purple),

extending into the twenty-first century under a high-emission scenario SSP585 (brown). Solid lines and shadings indicate multimodel mean and 95% confidence intervals on the basis of a Poisson distribution, respectively. The dashed black line indicates the mean level of piControl. **c**, As in part **a**, but for the *C*-index. **d**, As in part **b**, but for strong La Niña frequency. **e**, Multi-experiment mean *E*-index standard deviation for the 1901–1960 (green), 1961–2020 (purple) and 2041–2100 (brown) periods from each butterfly-effect large ensemble (LE) experiments and the multimodel ensemble average (MMEM). **f**, As in part **e**, but for the *C*-index. El Niño/Southern Oscillation variability progressively increases into the future, featuring an increasing frequency of strong El Niño and strong La Niña events.

spread owing to uncertainty in both signal and variability 43,63. However, changes in mean SST of the equatorial Pacific emerge earlier than in mean rainfall<sup>57</sup>. By contrast, changes in ENSO rainfall variability are projected to emerge earlier than changes in ENSO SST variability  $^{20,63}$ . Specifically, in the multimodel ensemble mean, without differentiating CP-ENSO from EP-ENSO, an ENSO rainfall variability signal emerges at about 2040 regardless of the emission scenario, some 30 years earlier than an ENSO SST variability signal which emerges at about 2070 (ref. 63). Assessing each of the two types of ENSO separately, increased EP-ENSO SST variability emerges from the piControl variability range around 2030 in ~70% of the models, more than a decade earlier than that of CP-ENSO<sup>43</sup>. The earlier emergence of EP-ENSO results from an increase in EP-ENSO rainfall response 12,14,45, which boosts the signal of increased SST variability, further enhanced by an ENSO-positive nonlinear atmospheric feedback<sup>43</sup>. The nonlinear Bjerknes feedback primarily operates in the eastern equatorial Pacific, where, once atmospheric deep convection is established, zonal winds increase nonlinearly with further warming<sup>3,50,64,65</sup>.

Measured against the distribution without greenhouse warming, post-1960 ENSO variability is unusually high, whereas the pre-1960 ENSO is not (Fig. 4). Indeed, the amplitude of the observed post-1960 *E*-index variability is within the highest 2.5th percentile. in sharp contrast to the pre-1960 E-index variability amplitude that sits below the 50th percentile (Fig. 4a). For the C-index, the observed amplitude of the post-1960 C-index variability sits between the highest 10th and 5th percentiles, with the pre-1960 C-index sitting around the 50th percentile (Fig. 4b). These post-1960 C-index changes are also unusual, but less so than the *E*-index, consistent with signals of ENSO change being more prominent in the *E*-index than in the *C*-index $^{43,50}$ . These features are also seen using a conventional ENSO index, with the post-1960 Niño3.4 sitting within the highest 5th to 10th percentiles, whereas the pre-1960 amplitude is around the 50th percentile (Supplementary Fig. 6). Thus, climate change has likely contributed to the observed post-1960 ENSO variability increase.

## **Explaining ENSO variability changes**

Collectively, these different approaches suggest a post-1960 increase in ENSO variance, likely attributed to anthropogenic warming. The projected increase in ENSO SST variability is not believed to be due to a change in the surface west-minus-east SST gradient  $^{50}$ . Although a faster warming in the eastern than in the western equatorial Pacific tends to be associated with a greater increase in ENSO SST variability, and vice versa  $^{66-68}$ , the faster warming in the east in part results from a rectification of the increase in ENSO SST variability onto the mean state  $^{67,69}$ .

Instead, the mechanism behind such an increase is similar to that responsible for the projected ENSO shifts, namely, changes in ocean

stratification. In response to increasing greenhouse gas emissions, the upper equatorial Pacific exhibits enhanced mean vertical stratification<sup>28,38,50</sup>: the near-surface ocean warms faster than the ocean below. The faster near-surface warming is a result of greenhouse gas-induced radiative forcing and increased precipitation-related freshening. Both enhance the response of the surface mixed layer to a given wind forcing<sup>50,70-72</sup>, strengthen ocean–atmosphere coupling<sup>50</sup> and contribute to a greater sensitivity of tropical Pacific SSTs to forcing from extratropical Pacific variability, even though its own variability does not necessarily change<sup>73</sup>.

From the pre-1960 to the post-1960 period, there is an intensification of the equatorial Pacific upper-ocean stratification that underpins the simulated ENSO change as a faster warming occurs near the surface than at the subsurface (Fig. 5a). These modelled vertical stratification changes are somewhat similar to the average of two reanalysis data sets<sup>74,75</sup> that have vertical ocean temperatures dating back to the 1950s and show an intensified vertical stratification (Supplementary information) (Fig. 5b). Statistically significant intermodel relationships exist: a greater enhancement in the vertical stratification is associated with a greater increase in E-index variability (Fig. 5c), which systematically translates into an increase in the frequency of strong El Niño (Fig. 5d). As a strong El Niño causes a large heat discharge, shallowing of the central Pacific thermocline that is conducive to La Niña, the increase in the frequency of strong El Niño, in turn, leads to more frequent strong La Niña events (Fig. 5e). The increase in the frequency of strong La Niña events thereby contributes to an enhanced C-index variability (Fig. 5f), despite the small reduction in central Pacific El Niño. The increased coupling means that positive feedbacks such as Ekman pumping, thermocline feedback and zonal advective feedbacks intensify<sup>1,76-79</sup>.

As reflected in the model simulations, rising CO<sub>2</sub> concentrations are a strong contributor to anthropogenic climate change. However, increasing CO<sub>2</sub> is not the only forcing factor; emissions of sulfur aerosols also increased since 1901 and then decreased from the mid-1980s back to the 1960 level by 2020. This decrease in aerosol emissions contributed to accelerated warming of the post-1960 period<sup>80</sup>, despite a continuous increase in emissions of other species that offset (organic carbon) or further enhance warming (black carbon)81. Butterfly-effect ensemble experiments, wherein single-forcing factors are separated, can be used to determine these isolated effects of aerosols and CO<sub>2</sub>. Although available in only two models, those simulations suggest that CO<sub>2</sub> has a large impact, but that a reduction in aerosols since the mid-1980s reinforced the conducive impact of increasing CO<sub>2</sub>, also intensifying upper ocean stratification of the equatorial Pacific, contributing to the post-1960 increase in ENSO variability<sup>82</sup>. These superimposing effects are likely to continue into the future.

## **Towards projected ENSO enhancement**

This evidence that anthropogenic warming has already enhanced post-1960 ENSO variability suggests that such changes are also integral to future projections. Indeed, a majority of the 43 models in the model democracy demonstrate further increases in the amplitude of the E-index, C-index and other indices under the SSP585 scenario (Supplementary Fig. 7). Specifically, comparisons of histograms of ensemble mean ENSO variability values over 60-year periods in the piControl experiments, 1961-2020 and 2041-2100 reveal progressively increasing EP-ENSO variability, with a value of 0.94, 1.03 and 1.17, respectively (Fig. 6a). The corresponding values for CP-ENSO are 0.95, 1.02 and 1.05, with a smaller increase in CP-ENSO up to 2041–2100 (Fig. 6c), again reinforcing that changes in EP-ENSO variability continue to be more detectable into the future<sup>43</sup>. The associated evolution of the frequency of strong El Niño and strong La Niña, averaged across all models, shows a general long-term increasing trend into 2100 (Fig. 6b,d). For example, strong El Niño frequency increases from 2.38 events per 60 years in the piControl to 4.13 events in 1961–2020 and 5.19 in 2041–2100. The corresponding strong La Niña frequency is 2.89, 4.11 and 4.57 events per 60 years for the 1901–1960, 1961–2020 and 2041–2100 periods, respectively. The increasing trend is not linear, likely modulated by factors including ENSO-rectified mean state fluctuations<sup>20,67</sup> and a differential mean warming rate between ocean basins19.

The projected trend towards ENSO enhancement seen in the model democracy approach might still be subject to residual influence of internal variability, particularly for the C-index owing to its weaker signal of increase. However, the continuous increase in ENSO variability is seen in multi-experiment means of the butterfly-effect ensembles, in which impact of internal variability is essentially removed; despite different emission scenarios, six out of seven ensemble means exhibit a continuous increase in *E*-index (Fig. 6e) and Niño3.4 variability (Supplementary Fig. 8) into the 2041–2100 period, and all seven models display an increase in C-index variability (Fig. 6f). Quantitatively, the large ensemble multimodel mean E-index variability values are 0.95, 1.05 and 1.18 standard deviations for the 1901–1960, 1961–2020 and 2041–2100 periods, respectively, with corresponding values of C-index variability of 0.96, 1.04 and 1.13 standard deviations. Similar findings hold if future ENSO variability is calculated over the 2021–2080 period (Supplementary Fig. 9). This strong intermodel consensus on increased C-index variability reinforces that signals of change in the C-index can be masked by internal variability<sup>43</sup>, but once much of internal variability is removed, the increase in C-index is prominent. The continuous increase reinforces that the post-1960 ENSO enhancement is likely a part of the long-term change.

#### Summary and future perspectives

In a single realization of the real world with limited observations, it is difficult, if not impossible, to determine whether observed ENSO has been affected by rising greenhouse gas emissions, even if quality of the available observation data was not an issue. However, model outputs from multicentury-long pre-industrial simulations of constant  $CO_2$  forcing, historical simulations forced with observed forcing and future simulations under emission scenarios offer a valuable resource to ascertain greenhouse gas forcing impact on ENSO.

A model democracy approach indicates that anthropogenic climate change has generated a statistically significant increase in ENSO SST variability between the pre-1960 and post-1960 period. This increased variability features more frequent occurrences of strong El Niño and strong La Niña events in the post-1960 period, but

little change in the CP El Niño frequency. The simulated increase in ENSO variability is also evident in seven large ensemble butterfly-effect experiments that remove the impact of internal variability. Moreover, 25,868 years of pre-industrial virtual climate further highlight that observed ENSO variability is unusually high in the post-1960 period. These simulated findings agree with palaeoclimatic evidence that ENSO variability in the twentieth century and early-twenty-first century is higher than in the distant past<sup>21,23,26</sup> and is consistent with projections suggesting continued and increasing ENSO SST variability in the future<sup>38,50</sup>. These changes in ENSO variability – both in the present and the future – are underpinned by an intensified upper ocean stratification of the equatorial Pacific. Collectively, this evidence suggests that the increase in observed ENSO variability post-1960 is at least in part related to anthropogenic warming.

There are additional research avenues to clarify the impact of climate change on observed ENSO. Although the data quality issue of historical SST is perpetual, a continuous search for new ENSO proxies offers potential to corroborate the findings on the basis of existing ENSO proxies of a high post-1960 ENSO variability<sup>21,23,25,26,82</sup>. Any extended or new proxies probably reflect a mixture of SST and signals such as hydroclimate or geochemistry rather than pure SST, but would add to the weight of available evidence. Emerging prospects include marine bivalves, which in the eastern and western tropical Pacific show a potential to track observed SST and capture ENSO variability<sup>83</sup>; marine sediments, which on the Peru margin display a history of flood events, arguably ENSO-driven<sup>84</sup>; and cave stalagmite records, which, in central America, contain an ENSO signal<sup>85</sup>. Future work on extending and identifying more locations with such ENSO-signal-carrying bivalve species, sediments and stalagmites offers a great potential.

In terms of climate model assessment, examination of simulated future change in additional ENSO properties, for example, ENSO onset, termination and seasonal phase locking, offers another pathway; a future change in any additional property of ENSO, if also seen in both the simulated and the observed post-1960 ENSO, would provide additional lines of evidence. Large ensemble of experiments under a single climate change forcing factor is currently available in a limited number of models only<sup>86</sup>. Given the effectiveness in reducing the intermodel spread and in quantifying the impact, such single-forcing large ensemble experiments performed in as many models as possible likely help separate the impact of CO<sub>2</sub>, aerosols and natural forcings such as volcanic eruptions, ultimately facilitating attribution of the post-1960 ENSO increase. Despite substantial improvement from previous generations, most CMIP models still under-estimate ENSO nonlinear Bjerknes feedback<sup>20,39</sup>. Nonlinear Bjerknes feedback amplifies ENSO response to greenhouse warming such that models simulating a greater feedback systematically generate a greater ENSO enhancement 39,43. Improved parameterization of atmospheric convection, cloud formation and their coupling to ENSO processes<sup>87</sup>, leading to a realistic nonlinear Bjerknes feedback, will potentially strengthen the simulated post-1960 ENSO enhancement and the intermodel consensus.

#### Data availability

Data relevant to the paper can be downloaded from 20CR v2c at https://portal.nersc.gov/project/20C\_Reanalysis/; CERA-20C at https://apps.ecmwf.int/datsets/dat/cera20c-edmo/levtype=sfc/type=an/; ERA-20C at https://apps.ecmwf.int/datsets/data/era20c-moda/levtype=sfc/type=an/; ERSST v3b at https://www.esrl.noaa.gov/psd/data/gridded/data.noaa.ersst.v3.html; HadISST v1.1 at https://www.esrl.noaa.gov/psd/data/gridded/data.hadsst.html;

COBE at https://psl.noaa.gov/data/gridded/data.cobe.html; ORA-s3 at http://apdrc.soest.hawaii.edu/datadoc/ecmwf\_oras3.php; ORA-s4 at https://climatedataguide.ucar.edu/climate-data/oras4-ecmwf-ocean-reanalysis-and-derived-ocean-heat-content and 111 CMIP6 database at https://esgf-node.llnl.gov/projects/cmip6/.

## Code availability

Codes for calculating EOF can be downloaded from: https://drive.google.com/open?id=1d2R8wKpFNW-vMlfoJsbqIGPIBd9Z 8rj.

Published online: 18 May 2023

#### References

- Kug, J. S., Jin, F. F. & An, S. I. L. Two types of El Niño events: cold tongue El Niño and warm pool El Niño. J. Clim. 22, 1499–1515 (2009).
- Kao, H. Y. & Yu, J. Y. Contrasting eastern-Pacific and central-Pacific types of ENSO. J. Clim. 22, 615–632 (2009).
- Takahashi, K., Montecinos, A., Goubanova, K. & Dewitte, B. ENSO regimes: reinterpreting the canonical and Modoki El Niño. Geophys. Res. Lett. 38, L10704 (2011).
- Takahashi, K. & Dewitte, B. Strong and moderate nonlinear El Niño regimes. Clim. Dyn. 46, 1627-1645 (2016).
- Capotondi, A. et al. Understanding ENSO diversity. Bull. Am. Meteorol. Soc. 96, 921–938
- Lengaigne, M. & Vecchi, G. A. Contrasting the termination of moderate and extreme El Niño events in coupled general circulation models. Clim. Dvn. 35, 299–313 (2010).
- Ropelewski, C. F. & Halpert, M. S. Global and regional scale precipitation patterns associated with the El Niño/Southern oscillation. *Mon. Weather Rev.* 115, 1606–1626 (1907)
- Bove, M. C., Eisner, J. B., Landsea, C. W., Niu, X. & O'Brien, J. J. Effect of El Niño on U.S. landfalling hurricanes, revisited. *Bull. Am. Meteorol. Soc.* 79, 2477–2482 (1998).
- 9. Bell, G. D. et al. Climate assessment for 1998. Bull. Am. Meteorol. Soc. 80, 1040 (1999).
- McPhaden, M. J., Zebiak, S. E. & Glantz, M. H. ENSO as an integrating concept in earth science. Science 314, 1740-1745 (2006).
- Cai, W. et al. Climate impacts of the El Niño-Southern oscillation on South America. Nat. Rev. Earth Environ. 1, 215–231 (2020).
- Cai, W. et al. Increasing frequency of extreme El Niño events due to greenhouse warming. Nat. Clim. Change 4, 111–116 (2014).
- Vincent, E. M. et al. Interannual variability of the South Pacific convergence zone and implications for tropical cyclone genesis. Clim. Dyn. 36, 1881–1896 (2011).
- Cai, W. et al. More extreme swings of the South Pacific convergence zone due to greenhouse warming. Nature 488, 365–369 (2012).
- Wang, G. et al. Future Southern ocean warming linked to projected ENSO variability. Nat. Clim. Change 12, 649–654 (2022).
- Cai, W. et al. Antarctic shelf ocean warming and sea ice melt affected by projected El Niño changes. Nat. Clim. Change 13, 235–239 (2023).
- Li, X. et al. Tropical teleconnection impacts on Antarctic climate changes. Nat. Rev. Earth Environ. 2, 680–698 (2021).
- Zhang, Q., Guan, Y. & Yang, H. ENSO amplitude change in observation and coupled models. Adv. Atmos. Sci. 25, 361–366 (2008).
- Kim, S. T. et al. Response of El Niño sea surface temperature variability to greenhouse warming. Nat. Clim. Change 4, 786-790 (2014).
- 20. Cai, W. et al. Changing El Niño-Southern oscillation in a warming climate. *Nat. Rev. Earth Environ.* **2**, 628–644 (2021).
- Grothe, P. R. et al. Enhanced El Niño-Southern oscillation variability in recent decades. Geophys. Res. Lett. 47, e2019GL083906 (2020).
- McGregor, S., Timmermann, A. & Timm, O. A unified proxy for ENSO and PDO variability since 1650. Clim. Past 6, 1–17 (2010).
- McGregor, S., Timmermann, A., England, M. H., Elison Timm, O. & Wittenberg, A. T. Inferred changes in El Niño-Southern oscillation variance over the past six centuries. Clim. Past 9, 2269–2284 (2013).
- Cobb, K. M. et al. Highly variable El Niño-Southern oscillation throughout the holocene. Science 339, 67-70 (2013).
- Karamperidou, C. et al. ENSO in a changing climate: challenges, paleo-perspectives, and outlook. in El Niño Southern Oscillation in a Changing Climate (eds McPhaden, M. J., Santoso, A. & Cai, W.) (AGU Monograph, 2020).
- Liu, Y. et al. Recent enhancement of central Pacific El Niño variability relative to last eight centuries. Nat. Commun. 8, 15386 (2017).
- Freund, M. et al. Higher frequency of Central Pacific El Niño events in recent decades relative to past centuries. Nat. Geosci. 12, 450–455 (2019).
- Collins, M. et al. The impact of global warming on the tropical Pacific ocean and El Niño. Nat. Geosci. 3, 391–397 (2010).
- DiNezio, P. N. et al. Mean climate controls on the simulated response of ENSO to increasing greenhouse gases. J. Clim. 25, 7399–7420 (2012).
- Dommenget, D. & Vijayeta, A. Simulated future changes in ENSO dynamics in the framework of the linear recharge oscillator model. Clim. Dyn. 53, 4233–4248 (2019).

- Stevenson, S. et al. Will there be a significant change to El Niño in the twenty-first century? J. Clim. 25, 2129–2145 (2012).
- Beobide-Arsuaga, G., Bayr, T., Reintges, A. & Latif, M. Uncertainty of ENSO-amplitude projections in CMIP5 and CMIP6 models. Clim. Dyn. 56, 3875–3888 (2021).
- Zheng, X. T., Hui, C. & Yeh, S. W. Response of ENSO amplitude to global warming in CESM large ensemble: uncertainty due to internal variability. Clim. Dyn. 50, 4019–4035 (2018).
- Maher, N., Matei, D., Milinski, S. & Marotzke, J. ENSO change in climate projections: forced response or internal variability? Geophys. Res. Lett. 45, 390–398 (2018).
- Gan, R., Liu, Q., Huang, G., Hu, K. & Li, X. Greenhouse warming and internal variability increase extreme and central Pacific El Niño frequency since 1980. Nat. Commun. 14, 394 (2023).
- Eyring, V. et al. Overview of the Coupled Model Intercomparison Project Phase 6 (CMIP6) experimental design and organization. Geosci. Model. Dev. 9, 1937–1958 (2016).
- Cai, W. et al. Increased frequency of extreme La Niña events under greenhouse warming. Nat. Clim. Change 5, 132–137 (2015).
- 38. Cai, W. et al. ENSO and greenhouse warming. Nat. Clim. Change 5, 849–859 (2015).
- Cai, W. et al. Increased ENSO sea surface temperature variability under four IPCC emission scenarios. Nat. Clim. Change 12, 228–231 (2022).
- Kennedy, J. J. A review of uncertainty in in situ measurements and data sets of sea surface temperature. Rev. Geophys. 52, 1–32 (2014).
- Gagan, M. K. Paleo-El Niño-Southern Oscillation (ENSO) Records. in Encyclopedia of Palaeoclimatology and Ancient Environments 721–728 (Springer, 2009).
- IPCC Climate Change: The Physical Science Basis (eds Masson-Delmotte, V. et al.) (Cambridge Univ. Press, 2021).
- Geng, T. et al. Emergence of changing Central-Pacific and Eastern-Pacific El Niño-Southern Oscillation in a warming climate. Nat. Commun. 13, 6616 (2022).
- Santoso, A. et al. Late-twentieth-century emergence of the El Niño propagation asymmetry and future projections. Nature 504, 126 (2013).
- Power, S. B., Delage, F., Chung, C., Kociuba, G. & Keay, K. Robust twenty-first century projections of El Niño and related precipitation variability. Nature 502, 541–545 (2013).
- Wang, G. et al. Continued increase of extreme El Niño frequency long after 1.5°C warming stabilization. Nat. Clim. Change 7, 568–572 (2017).
- Brown, J. R. et al. South Pacific convergence zone dynamics, variability and impacts in a changing climate. Nat. Rev. Earth Environ. 1, 530–543 (2020).
- Yun, K. S. et al. Increasing ENSO-rainfall variability due to changes in future tropical temperature-rainfall relationship. Commun. Earth Environ. 2, 43 (2021).
- McPhaden, M. J., Santoso, A., & Cai, W. (eds) El Niño Southern Oscillation in a Changing Climate Vol. 253 (John Wiley & Sons, 2020).
- Cai, W. et al. Increased variability of eastern Pacific El Niño under greenhouse warming. Nature 564, 201-206 (2018).
- Taylor, K. E., Stouffer, R. J. & Meehl, G. A. An overview of CMIP5 and the experiment design. Bull. Am. Meteorol. Soc. 93, 485–498 (2012).
- Fredriksen, H.-B., Berner, J., Subramanian, A. C. & Capotondi, A. How does El Niño-Southern oscillation change under global warming — a first look at CMIP6. Geophys. Res. Lett. 47, e2020GL090640 (2020).
- Wittenberg, A. T. Are historical records sufficient to constrain ENSO simulations? Geophys. Res. Lett. 36, L12702 (2009).
- Stevenson, S. L. Significant changes to ENSO strength and impacts in the twenty-first century: results from CMIP5. Geophys. Res. Lett. 39, L17703 (2012).
- Ng, B., Cai, W., Cowan, T. & Bi, D. Impacts of low-frequency internal climate variability and greenhouse warming on El Niño-Southern oscillation. J. Clim. 34, 2205–2218 (2021).
- Cai, W. et al. Butterfly effect and a self-modulating El Niño response to global warming. Nature 585, 68-73 (2020).
- Hawkins, E. & Sutton, R. Time of emergence of climate signals. Geophys. Res. Lett. 39, L01702 (2012).
- 58. Deser, C. et al. Insights from Earth system model initial-condition large ensembles and future prospects. *Nat. Clim. Change* **10**, 277–286 (2020).
- Deser, C. et al. ENSO and Pacific decadal variability in the Community Climate System Model version 4. J. Clim. 25, 2622–2651 (2012).
- Hawkins, E., Smith, R. S., Gregory, J. M. & Stainforth, D. A. Irreducible uncertainty in near-term climate projections. Clim. Dyn. 46, 3807–3819 (2016).
- Machete, R. L. & Smith, L. A. Demonstrating the value of larger ensembles in forecasting physical systems. *Tellus A Dyn. Meteorol. Oceanogr.* 68, 28393 (2016).
- Bengtsson, L. & Hodges, K. I. Can an ensemble climate simulation be used to separate climate change signals from internal unforced variability? Clim. Dyn. 52, 3553–3573 (2019).
- Ying, J. et al. Emergence of climate change in the tropical Pacific. Nat. Clim. Change 12, 356–364 (2022).
- Geng, T., Cai, W. & Wu, L. Two types of ENSO varying in tandem facilitated by nonlinear atmospheric convection. Geophys. Res. Lett. 47, e2020GL088784 (2020).
- Geng, T., Cai, W., Wu, L. & Yang, Y. Atmospheric convection dominates genesis of ENSO asymmetry. Geophys. Res. Lett. 46, 8387–8396 (2019).
- Zheng, X.-T., Xie, S.-P., Lv, L. H. & Zhou, Z. Q. Intermodel uncertainty in ENSO amplitude change tied to Pacific Ocean warming pattern. J. Clim. 29, 7265–7279 (2016).
- Hayashi, M., Jin, F.-F. & Stuecker, M. F. Dynamics for El Niño-La Niña asymmetry constrain equatorial-Pacific warming pattern. Nat. Commun. 11, 4230 (2020).
- Ying, J., Huang, P., Lian, T. & Chen, D. Intermodel uncertainty in the change of ENSO's amplitude under global warming: role of the response of atmospheric circulation to SST anomalies. J. Clim. 32, 369–383 (2019).

- Kohyama, T., Hartmann, D. L. & Battisti, D. S. La Niña-like mean-state response to global warming and potential oceanic roles. J. Clim. 30, 4207-4225 (2017).
- Carréric, A. et al. Change in strong Eastern Pacific El Niño events dynamics in the warming climate. Clim. Dyn. 54, 901–918 (2020).
- Dewitte, B., Yeh, S.-W., Moon, B.-K., Cibot, C. & Terray, L. Rectification of the ENSO variability by interdecadal changes in the equatorial background mean state in a CGCM simulation. J. Clim. 20, 2002–2021 (2007).
- Thual, S., Dewitte, B., An, S.-I. & Ayoub, N. Sensitivity of ENSO to stratification in a recharge-discharge conceptual model. J. Clim. 4, 4331–4348 (2011).
- Jia, F., Cai, W., Gan, B., Wu, L. & Di Lorenzo, E. Enhanced north Pacific impact on El Niño/Southern Oscillation under greenhouse warming. Nat. Clim. Change 11, 840–847 (2021)
- Balmaseda, M. A., Vidard, A. & Anderson, D. L. T. The ECMWF ocean analysis system: ORA-S3. Mon. Weath Rev. 136. 3018–3034 (2008).
- Balmaseda, M. A., Mogensen, K. & Weaver, A. T. Evaluation of the ECMWF ocean reanalysis system ORAS4. Q. J. R. Meteorol. Soc. 139, 1132–1161 (2013).
- Jin, F.-F. An equatorial ocean recharge paradigm for ENSO. Part I: conceptual model. J. Atmos. Sci. 54, 811–829 (1997).
- Fang, X. & Mu, M. A three-region conceptual model for central Pacific El Niño including zonal advective feedback. J. Clim. 31, 4965–4979 (2018).
- Chen, N., Fang, X. & Yu, J. Y. A multiscale model for El Niño complexity. npj Clim. Atmos. Sci. 5, 16 (2022).
- Fang, X. & Chen, N. Quantifying the predictability of ENSO complexity using a statistically accurate multiscale stochastic model and information theory. J. Clim. 36, 2681–2702 (2023).
- IPCC Climate Change 2013: The Physical Science Basis. Contribution of Working Group I to the Fifth Assessment Report of the Intergovernmental Panel on Climate Change (eds Stocker, T. F. et al.) 1535 pp. (Cambridge Univ. Press, 2013).
- Hoesly, R. M. et al. Historical (1750–2014) anthropogenic emissions of reactive gases and aerosols from the Community Emissions Data System (CEDS). Geosci. Model. Dev. 11, 369–408 (2018).
- Emile-Geay, J. et al. Past ENSO variability: reconstructions, models, and implications.
  In El Niño Southern Oscillation in a Changing Climate (eds McPhaden, M. J., Santoso, A. & Cai, W.) (AGU Monograph, 2020).
- Carre, M., Sachs, J. P., Schauer, A. J., Rodriguez, W. E. & Ramos, F. C. Reconstructing El Niño-Southern oscillation activity and ocean temperature seasonality from short-lived marine mollusk shells from Peru. *Palaeogeogr. Palaeoclimatol. Palaeoecol.* 371, 45–53 (2013).
- Rein, B. How do the 1982/83 and 1997/98 El Niño's rank in a geological record from Peru? Quat. Int. 161. 56–66 (2007).
- Frappier, A., Sahagian, D., Gonzalez, L. A. & Carpenter, S. J. El Niño events recorded by stalagmite carbon isotopes. Science 298, 565–565 (2002).
- Maher, N. et al. The future of the El Niño-Southern oscillation: using large ensembles to illuminate time-varying responses and inter-model differences. Earth Syst. Dyn. Discuss https://doi.org/10.5194/esd-2022-26 (2022).
- Bony, S. & Dufresne, J. L. Marine boundary layer clouds at the heart of tropical cloud feedback uncertainties in climate models. Geophys. Res. Lett. 32, L20806 (2005).
- Compo, G. P. et al. The twentieth century reanalysis project. Q. J. R. Meteorol. Soc. 137, 1–28 (2011).
- Laloyaux, P. et al. CERA-20C: a coupled reanalysis of the twentieth century. J. Adv. Model. Earth Syst. 10, 1172–1195 (2018).

- Poli, P. et al. ERA-20C: an atmospheric reanalysis of the twentieth century. J. Clim. 29, 4083–4097 (2016).
- Smith, T. M., Reynolds, R. W., Peterson, T. C. & Lawrimore, J. Improvements to NOAA's historical merged land-ocean surface temperature analysis (1880–2006). J. Clim. 21, 2283–2296 (2008).
- Rayner, N. A. et al. Global analyses of sea surface temperature, sea ice, and night marine air temperature since the late nineteenth century. J. Geophys. Res. 108, 4407 (2003).
- Ishii, M., Shouji, A., Sugimoto, S. & Matsumoto, T. Objective analyses of sea-surface temperature and marine meteorological variables for the 20th century using ICOADS and the Kobe collection. *Int. J. Climatol.* 25, 865–879 (2005).

#### **Acknowledgements**

This project is supported by the Science and Technology Innovation Project of Laoshan Laboratory (LSKJ202203300) and the Strategic Priority Research Programme of Chinese Academy of Sciences (XDB 40030000) TG is supported by the National Natural Science Foundation of China (NSFC) project (42206209, 42276006) and China National Postdoctoral Program for Innovative Talents (BX20220279), L.W., X.L. and B.G. are supported by the NSFC projects (41490643, 41490640, U1606402 and 41521091). W.C., G.W., B.N. and A.S. are supported by CSHOR, a joint research Center for Southern Hemisphere Oceans Research between QNLM and CSIRO. A.S., B.N. and G.W. are supported by the Australian Government's National Environmental Science Program (NESP). M.C. was supported by a grant from the UK  $Natural\ Environment\ Research\ Council\ (NE/S004645/1).\ The\ authors\ acknowledge\ the\ World$ Climate Research Programme's Working Group on Coupled Modelling, which is responsible for CMIP, and the authors thank the climate modelling groups for producing and making available their model output. For CMIP, the US Department of Energy's Program for Climate Model Diagnosis and Intercomparison provides coordinating support and led development of software infrastructure in partnership with the Global Organization for Earth System Science Portals. The authors are also grateful to various reanalysis groups for making the data sets available to us. PMEL contribution no. 4957.

#### **Author contributions**

W.C. conceived the article and wrote the initial manuscript in discussion with T.G., B.N. and L.W. B.N. and T.G. performed analysis and generated final figures. All authors contributed to interpreting findings, discussion of the associated dynamics and improvement of this paper.

#### **Competing interests**

The authors declare no competing interests.

### Additional information

**Supplementary information** The online version contains supplementary material available at https://doi.org/10.1038/s43017-023-00427-8.

**Peer review information** *Nature Reviews Earth & Environment* thanks Xiang-Hui Fang, Ping Huang and the other, anonymous, reviewer(s) for their contribution to the peer review of this work.

**Publisher's note** Springer Nature remains neutral with regard to jurisdictional claims in published maps and institutional affiliations.

© Crown 2023

<sup>1</sup>Frontier Science Center for Deep Ocean Multispheres and Earth System and Key Laboratory of Physical Oceanography, Ocean University of China, Qingdao, China. <sup>2</sup>Center for Southern Hemisphere Oceans Research (CSHOR), CSIRO Oceans and Atmosphere, Hobart, TAS, Australia. <sup>3</sup>Laoshan Laboratory, Qingdao, China. <sup>4</sup>Key Laboratory of Ocean Circulation and Waves, Institute of Oceanology, Chinese Academy of Sciences, Qingdao, China. <sup>5</sup>The State Key Laboratory of Loess and Quaternary Geology, Institute of Earth Environment, Chinese Academy of Sciences, Xi'an, China. <sup>6</sup>State Key Laboratory of Numerical Modeling for Atmospheric Sciences and Geophysical Fluid Dynamics, Institute of Atmospheric Physics, Chinese Academy of Sciences, Beijing, China. <sup>7</sup>Australian Research Council (ARC) Center of Excellence for Climate Extremes, University of New South Wales, Sydney, NSW, Australia. <sup>8</sup>College of Global Change and Earth System Science, Beijing Normal University, Beijing, China. <sup>9</sup>Department of Atmospheric Science, SOEST, University of Hawaii at Manoa, Honolulu, Hawaii, USA. <sup>10</sup>Department of Mathematics and Statistics, University of Exeter, Exeter, UK. <sup>11</sup>NOAA/Pacific Marine Environmental Laboratory, Seattle, WA, USA.